Machine Learning-based Diesel Engine-Out NOx Reduction Using a plug-in PD-type Iterative Learning Control

Armin Norouzi*, David Gordon*, Masoud Aliramezani*, Charles Robert Koch*

***Abstract*— A plug-in Iterative Learning Controller (ILC) is proposed to reduce the engine-out Oxides of Nitrogen (NOx) emissions of a medium-duty diesel engine. A control-oriented model is developed to simulate the dynamic behavior of NOx, Carbon Monoxide (CO), and unburned hydrocarbon (UHC) emissions as well as engine power output given by the break mean effective pressure (BMEP). This control-oriented model consists of a support vector machine (SVM) that calculates the steady-state values of the emissions and BMEP as a function of the engine speed, the amount of injected fuel and the injection rail pressure. The SVM-based model was then augmented using experimental results from a fast response electrochemical NOx sensor to predict the transient behavior of the engine. Finally, a plug-in PD-type ILC that consists of a PID and an ILC controller is developed to reduce the amount of engine-out NOx while controlling the desired engine power, represented by BMEP, and monitoring the other emissions. The proposed controller provides a powerful tool for engine-out emissions trade-off in addition to controlling the desired engine output power.**

***Index Terms*— Iterative Learning Control, Diesel Engine, Emission Control, Internal Combustion Engine Control, Plug-in Learning Control, Machine Learning, Support Vector Machine**

I. INTRODUCTION

Iterative learning control (ILC) is used to improve the tracking performance of systems with a repetitive reference or disturbance. Often off-highway equipment is subjected to the same repetitive load cycle through its normal daily operation. The main advantage of ILC is the ability to learn from tracking error present in the previous cycle to improve the tracking of the current cycle. This results in a non-causal controller that is able to predict changes in the upcoming control output [1], [2]. The simple structure of ILC makes it reliable, computationally inexpensive, and easy to design and thus ideal for real-time implementation [3]. ILC has some unique advantages over classic, non-linear, and model-based control methods and can also be used in conjunction these classical controllers.

ILC was first used in 1984 [4] and since then ILC has been used for various cyclic systems. When combined with traditional controllers, P-type, PD-type and PID-type ILC has been used successfully used [5], [6], [7]. The plant inversion method allows for the design of a switched ILC (SILC) controller for MIMO systems [8]. Both Adaptive and Fuzzy controllers have been combined with ILC and has been shown to improve ILC performance [9], [10]. When N-parametric type ILC is applied to SISO linear time-invariant (LTI) systems the optimal controller gain can be determined [11].

The high fuel efficiency and torque output of diesel engines has lead to their use for production of mechanical power for decades [12]. The benefits of the diesel engine has resulted in their use in a variety of applications including on-road and off-highway use in both the heavy-duty and light-duty sectors as well as for stationary power generation. However, the non-homogeneous air-fuel mixture and the use of diffusion combustion results in increased NO_x and particulate matter emissions [13]. Different combustion strategies have been experimentally tested to address this challenge and reduce engine-out NO_x emissions including Exhaust Gas Recirculation (EGR) [14], Low Temperature Combustion (LTC) [15] and various injection strategies[16]. Exhaust gas after-treatment systems have also been developed to reduce NO_x such as the urea-based Selective Catalytic Reduction (SCR) [17].

Controller implementations such as gain scheduling [18] and model predictive control (MPC) [19] have been shown to provide NO_x reduction benefits. However, both of these controller implementations require an accurate system model and variations in the system over time are difficult to model. ILC provides a model free controller method that is also able to learn changes in the system over time.

With the implementation of real driving emissions (RDE) legislation and the emission reduction targets becoming evermore stringent new engine control strategies and real-time emissions sensors are needed to meet NO_x regulations [20]. Fast response engine emission sensors for engine feedback control [21] are vital in being able to meet the strict emission regulations [22] and carrying out on-board diagnostics [23].

This work focuses on improving the engine-out emissions of a 4-cylinder diesel engine. A plug-in type ILC with a conventional PID controller will be used with an emissions model for the reduction of NO_x engine out emissions of a stationary diesel engine.

II. EXPERIMENTAL SETUP

A. Diesel Engine

A 4-cylinder medium duty diesel engine (Cummins QSB4.5 160) is used for model development in this work. This engine is Tier 3 certified and traditionally used for stationary off-highway applications [24].

*Mechanical Engineering Department, Faculty of Engineering, University of Alberta, 116 St & 85 Ave, Edmonton, AB, Canada norouziy@ualberta.ca, dgordon@ualberta.ca, aliramez@ualberta.ca, bob.koch@ualberta.ca

B. Electrochemical NO_x sensor

A fast response amperometric NO_x sensor (ECM-06-05) is used to capture the emission transients. An after-market sensor control module (*ECM-NOxCANt* P/N: 02-07) is used to set the sensor working parameters via a CAN interface (*Kvaser Light HS*).

C. Fourier-Transform Infrared Spectroscopy (FTIR)

A FTIR analyser (*MultiGas 2030*) was used to validate the ECM NO_x sensor measurement and to measure the concentration of other emissions (CO and UHC) in the exhaust gas. The FTIR analyser was connected to the diesel engine exhaust pipe, to measure the engine-out emissions. To avoid water vapor condensation in the sample lines, they were heated to 191^{o}C. The sample exhaust gas passes through two heated filters (*Flexotherm Flex*) before going to the FTIR.

The experimental setup of diesel engine is schematically shown in Fig. 1.

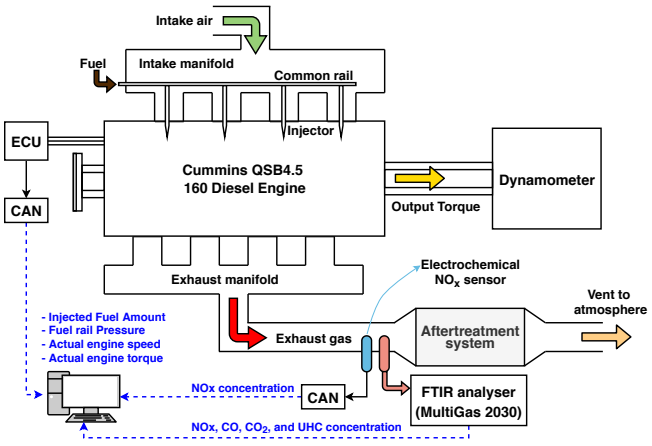

Fig. 1. Experiment setup - medium duty diesel Engine

III. DIESEL ENGINE EMISSION AND PERFORMANCE MODELING

In this study, a previously developed support vector machine (SVM) based control-oriented model is used to predict the engine out NO_x and BMEP [25]. A CO and UHC model has been developed using same structure and will be discussed in this section.

A. NO_x and BMEP steady-state model

The SVM model for NO_x and BMEP is developed using 84 experimental data points at different engine operating conditions. The inputs (features) of the SVM model are selected based on a combination of fuel rail pressure (P_r-$[bar]$), injected fuel amount (m_f - $[mg/stroke]$) and engine speed (n -$[rpm]$) as proposed in [25]. The SVM regression model for steady state NO_x and BMEP is then defined as:

$$\mathbf{x_{ss}} = \mathbf{w}^T \bar{u} + \mathbf{b} \tag{1}$$

where, $\mathbf{x_{ss}} = [NO_{x,ss} \quad BMEP_{ss}]^T$, matrices w and b are obtained by solving the SVM algorithm [25]. Vector $\bar{u}$ is the polynomial feature space which is found based on a correlation-based model order reduction strategy [25].

B. UHC and CO steady-state model

Using the same technique as the NO_x model above, a steady state SVM-based CO-UHC model is developed. The model is based on 13 experimental data points where 11 points are used to train the model and 2 points are reserved for testing. The feature set is defined as

$$\begin{aligned} &u_1 = m_f, \quad u_2 = n, \quad u_3 = p_r, \quad , u_4 = m_f^2, \quad u_5 = n^2 \\ &u_6 = p_r^2, \quad u_7 = m_f n, \quad u_8 = m_f p_r, \quad u_9 = n p_r \end{aligned} \tag{2}$$

where P_r $[bar]$ is fuel rail pressure, m_f $[mg/stroke]$ is the injected fuel amount, and $[n\ rpm]$ is the engine speed.

By solving the SVM algorithm for the training data set the approximate function, $\mathbf{x_{ss}}$ is obtained to model the steady-state values of COand UHC as

$$\begin{aligned} CO_{ss} &= 11.50\bar{u}_1 + 19.07\bar{u}_2 - 21.84\bar{u}_3 + 22.37\bar{u}_4 \\ &\quad - 28.46\bar{u}_5 - 8.19\bar{u}_6 - 69.39\bar{u}_7 - 26.56\bar{u}_8 \\ &\quad + 31.43\bar{u}_9 + 206.35 \\ UHC_{ss} &= -10.84\bar{u}_1 + 7.03\bar{u}_2 + 9.80\bar{u}_3 + 14.30\bar{u}_4 \\ &\quad + 4.03\bar{u}_5 - 6.94\bar{u}_6 - 15.84\bar{u}_7 + 1.37\bar{u}_8 \\ &\quad - 9.99\bar{u}_9 + 12.22 \end{aligned} \tag{3}$$

where CO_{ss} and UHC_{ss} are the steady-state CO and UHC concentrations [ppm]. $\bar{u}$ is the vector of normalized features. The developed emission models are compared with an Artificial Neural Network (ANN) model with two hidden layers. The coefficient of determination, R^2, for the UHC model is 0.8988 and 0.8566 for the ANN and SVM models, respectively. For the CO model a R^2 value of 0.9422 and 0.9733 is obtained for the ANN and SVM models. The R^2 value for both models are very close, however, the linear kernel used in SVM results in a simple mathematic equation. This allows for the implementation of a real-time observer when the SVM model is used. Finally, convergence to the global minimum is guaranteed when using SVM. However, ANN (which uses the gradient descent learning algorithm) tends to converge to a local minima. As a result, it can suffer from over-fitting [26].

C. Emission and performance control-oriented model

The effect of engine dynamics on the transient emissions and performance are approximated using a simple first order lag which is defined as

$$x_t(s) = \frac{1}{\tau s + 1} x_{ss}(s) \tag{4}$$

where, $x_t(s)$ is the transient variable and $x_{ss}(s)$ is the steady state variable, all in the Laplace domain. τ is a time constant for NO_x and BMEP, and is calculated based on the experimental data to be 1 second and 0.2 seconds, respectively [24], [27]. As no real-time measurement of CO or UHC is available, it is assumed that the time constants of all gaseous emissions are the same as the NO_x measurement. Therefore, the same value of time constant is used for NO_x,

UHC, and CO. To derive the discrete control-oriented model, the first order lags are written in z-transform using backward Euler method (implicit Euler method) as

$$X_t(z) = \frac{T}{T + \tau - \tau z^{-1}} X_{ss}(z) \tag{5}$$

where T is the sampling interval. Therefore, the discrete-time control-oriented model is achieved as

$$x(k) = A_k x(k-1) + B_k u(k), \quad y(k) = C_k x(k) \tag{6}$$

where

$$\mathbf{A_k} = \begin{bmatrix} \frac{\tau_{BMEP}}{\tau_{BMEP}+T} & 0 & 0 & 0 \\ 0 & \frac{\tau_{NO_x}}{\tau_{NO_x}+T} & 0 & 0 \\ 0 & 0 & \frac{\tau_{CO}}{\tau_{CO}+T} & 0 \\ 0 & 0 & 0 & \frac{\tau_{UHC}}{\tau_{UHC}+T} \end{bmatrix}$$

$$\mathbf{B_k} = \begin{bmatrix} \frac{T}{\tau_{BMEP}+T} & 0 & 0 & 0 \\ 0 & \frac{T}{\tau_{NO_x}+T} & 0 & 0 \\ 0 & 0 & \frac{T}{\tau_{CO}+T} & 0 \\ 0 & 0 & 0 & \frac{T}{\tau_{UHC}+T} \end{bmatrix}$$

$$\mathbf{C_k} = \begin{bmatrix} 1 \\ 1 \\ 1 \\ 1 \end{bmatrix}^T, \ \mathbf{x} = \begin{bmatrix} BMEP \\ \mathrm{NO_x} \\ CO \\ UHC \end{bmatrix}, \ \mathbf{u} = \begin{bmatrix} BMEP_{ss} \\ NO_{x,ss} \\ CO_{ss} \\ UHC_{ss} \end{bmatrix}$$

This transient model appears to decouple the $\mathrm{NO_x}$ and BMEP models; however, the transient model is dependent on the steady-state model outputs. As the steady state $\mathrm{NO_x}$ and BMEP models use the same inputs they are actually highly coupled. The transient results for $\mathrm{NO_x}$, BMEP, CO and UHC are shown in Figure 2.

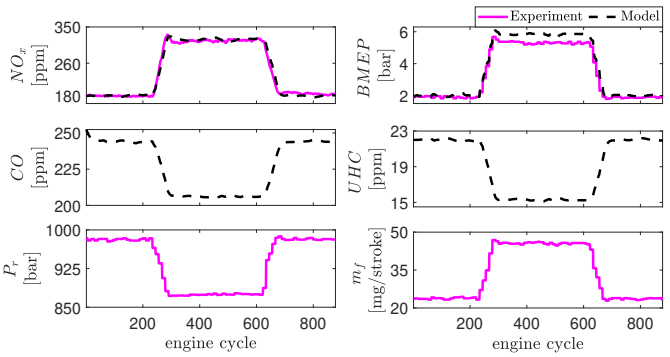

Fig. 2. Open loop model response for experimental rail pressure and injected fuel amount input

IV. CONTROL STRATEGY

A. ITERATIVE LEARNING CONTROLLER

The ILC control law is generally defined as

$$u_{j+1}(k) = Q(u_j(k)) + L(e_j(k)) \tag{7}$$

where L-filter is a learning operator and Q-filter is a control input filter, k represent discrete time index which is defined from k = 0 to k = N which results in a cycle period of $\tau = NT_s$, where T_s is the sample time. The index j represents the iteration cycle. The P-type ILC controller is the simplest type of ILC controller where the Q-filter is equal to the identity matrix and L-filter is a constant matrix. The P-type ILC controller is defined as

$$u_{j+1}(k) = u_j(k) + Pe_j(k) \tag{8}$$

where P is a proportional gain or in general a constant matrix. Additionally, by adding a derivative term to the L-filter, the PD-type ILC controller is obtained. The PD-type control law is defined as

$$u_{j+1}(k) = u_j(k) + Pe_j(k) + \hat{D}\big(\frac{e_j(k) - e_j(k-1)}{T_s}\big) \tag{9}$$

where p and D are the proportional and derivative learning gain respectively. The discretization sampling time is defined as T_s. By defining $\hat{D} = D/T_s$, the PD-type ILC is rewritten as

$$u_{j+1}(k) = u_j(k) + Pe_j(k) + D(e_j(k) - e_j(k-1)) \tag{10}$$

Using the z-transform properties and assuming zero initial conditions, the PD-type ILC control law in the z domain is obtained as:

$$U_{j+1}(z) = U_j(z) + PE_j(z) + D\frac{1}{1 - z^{-1}} E_j(z) \tag{11}$$

B. PLUG-IN TYPE OF ILC CONTROLLER

ILC control can be combined with conventional control as shown in Fig. 3. The conventional control is added as "plug-in". For the plug-in type learning control, the previous cycle error and ILC control input are added to a conventional control output as shown in Fig. 3. The PID gains of the conventional controller are held constant throughout the testing and only the ILC output is varied based on the previous error and control signals. The conventional control can be selected as needed such as a PID controller or nonlinear control method such as an advanced sliding mode controller [28]. The plug-in PD-type ILC with parallel structure is given by

$$U_j(z) = U_{ILC,j}(z) + U_{c,j}(z) \tag{12}$$

where $U_{c,j}(z)$ is the conventional controller output, $U_{j,ILC}(z)$ is the ILC output and $U_j(z)$ is the control signal of the system. In this study a discrete-time PID controller (using backward method) is used as

$$U_{c,j}(z) = \big(K_p + \frac{K_i}{1 - z^{-1}} + K_d(1 - z^{-1})\big) E_j(z) \tag{13}$$

where K_p, K_i, and K_d are the conventional PID controller gains. Adding the ILC controller to a conventional controller improves the system robustness to both the uncertainty of the system and any periodic external disturbances. Setting (tuning) of the conventional controller gains - here the PID gains - are also easier. The control input from the ILC control is based on the previous cycle error while the control input from the PID controller is based on the current cycle error and fixed PID coefficients. Another advantage of adding the

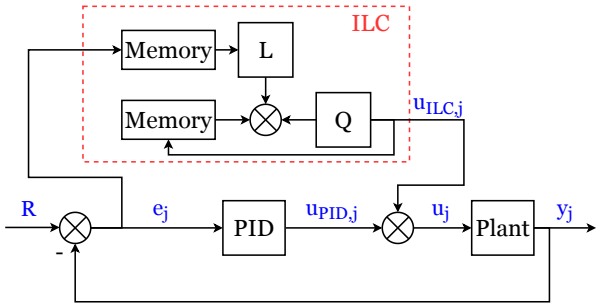

Fig. 3. Plug-in Iterative Learning Controller with parallel structure

embedded control is model mismatch compensation. The model mismatch occurs due to using the linearization of complex non-linear model for control design [29], [30].

In this study the plug-in PD-type ILC controller is used for tracking of a desired set point for diesel engine-out NO_x and BMEP using the model described in the previous section. Both the PID and the plug-in PD-type ILC controller are tested in simulation. Here, the control variables are fuel rail pressure and injected fuel amount and the manipulated variables are BMEP, NO_x, CO, and UHCand the engine speed is set to be constant at 1500 rpm. The results of the plug-in PD-type ILC with PID controller with respect to the pure PID controller is shown in Fig. 4. Additionally, convergence of the plug-in PD-type ILC controller is shown by plotting the Euclidean norm of the cycle error with respect to the number of iterations. Based on the Fig. 4, the plug-in PD-type ILC takes advantage of both the ILC and PID controllers to track the desired reference. The ILC plug-in controller improves the convergence time when compared to the pure PID controller.

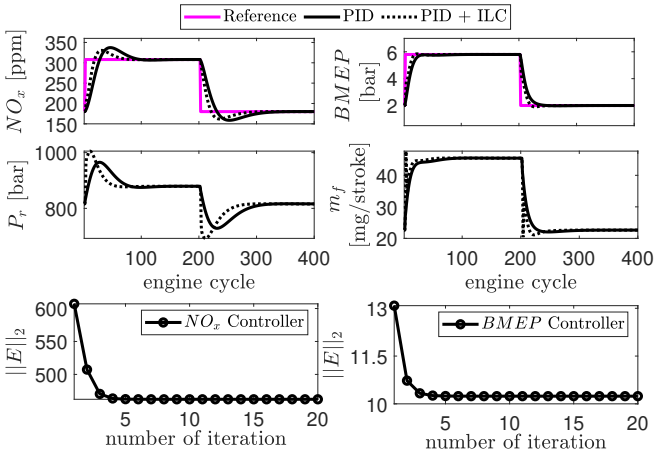

Fig. 4. PID controller vs plug-in PID and PD-type ILC controller

C. STABILITY ANALYSIS OF CONTROLLER

To analyze the stability and convergence of the P-type ILC, the term $Q - LG$ is considered as the criteria, where G is open loop system transfer function. The P-type ILC stability and monotonic convergence are defined as

- The necessary but not sufficient conditions for P-type ILC asymptotic stability is $|Q - GL||_\infty < 1$ or maximum singular value of $[Q - GL]$ is less than one [31].
- The monotonic convergence of $e_{j+1} = Me_j$ with $M = [Q - G(z)L]$ occurs when using the Euclidean norm and when the maximum singular value less than one as $\bar{\sigma}(M) < 1$

It can be shown that for the PD-type ILC, M is calculated as $M = [I - G(z)(P + \frac{D}{1-z^{-1}})]$. Using this definition, the asymptotic stability and monotonic convergence condition is obtained as $\bar{\sigma}(I - G(z)(P + \frac{D}{1-z^{-1}})) < 1$ [30].

Now, the stability and convergence criteria for the plug-in PD-type ILC for single-input single-output (SISO) system can be calculated. Therefore, M for the plug-in PD-type ILC controller is obtained using Eqs. 13 and 11 as

$$\begin{aligned} E_{j+1}(z) &= R(z) - Y_{j+1}(z) = R(z) - G(z)u_{j+1}(z) \\ &= R(z) - G(z)\big(K_p + \frac{K_i}{1-z^{-1}} \\ &+ K_d(1-z^{-1})\big)E_{j+1}(z) - G(z)\big(U_j(z) \\ &+ PE_j(z) + \frac{D}{1-z^{-1}}E_j(z)\big) \end{aligned} \tag{14}$$

By substituting $E_j(z) = R(z) - G(z)U_j(z)$ into Eq. 14 and factoring out of $E_j(z)$ and $E_{j+1}(z)$, we have

$$\begin{aligned} &E_{j+1}(z)(1 + G(z)\big(K_p + \frac{K_i}{1-z^{-1}} + K_d(1-z^{-1})\big) \\ &= \big(1 - G(z)PE_j(z) - G(z)\frac{D}{1-z^{-1}}\big)E_j(z) \end{aligned} \tag{15}$$

As $E_{j+1}(z) = ME_j(z)$, M is calculated as

$$M = \frac{a_0 + a_1 z^{-1}}{b_0 + b_1 z^{-1} + b_2 z^{-2}} \tag{16}$$

where

$$\begin{aligned} &a_0 = 1 + G(z)(P + D),\ a_1 = -1 - G(z)P \\ &b_0 = 1 - G(z)(K_i + K_d),\ b_1 = -1 - G(z)(K_p + 2K_d) \\ &b_2 = -G(z)K_d \end{aligned}$$

So, the asymptotic stability and monotonic convergence condition is obtained as

$$\bar{\sigma}\Big(\frac{a_0 + a_1 z^{-1}}{b_0 + b_1 z^{-1} + b_2 z^{-2}}\Big) < 1 \tag{17}$$

In this study, controller gains have been set to satisfy asymptotic stability and monotonic convergence of controller based on Eq. 17.

V. RESULTS AND DISCUSSIONS

The developed PD-type ILC controller is then tested in simulation to determine the potential NO_x reduction and the resulting impact on the other emissions. The simulated controller output is compared to the measured engine emissions levels. A cycle of 4 load steps (4.7, 6.6, 10.4 and 12.3 bar BMEP) is used to represent the uptake of load by the engine. This cycle could be modified to match the actual load cycle experienced in specific engine applications.

The emission model described earlier in this work is then used to simulate the system response. The ILC controller is

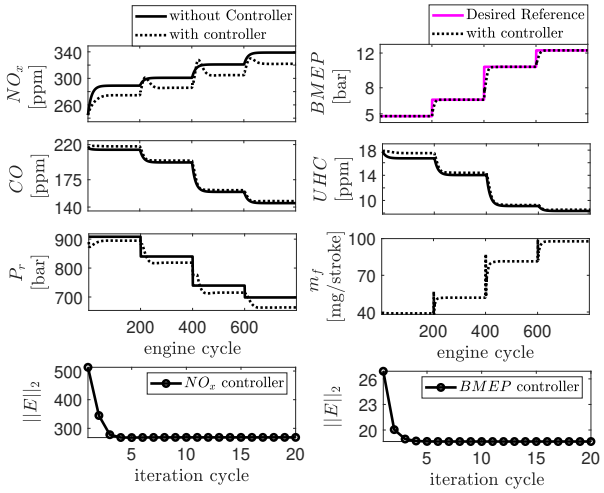

Fig. 5. NO_x Reduction system using plug-in PID and PD-type ILC - desired to reduce NO_x by 5 percent

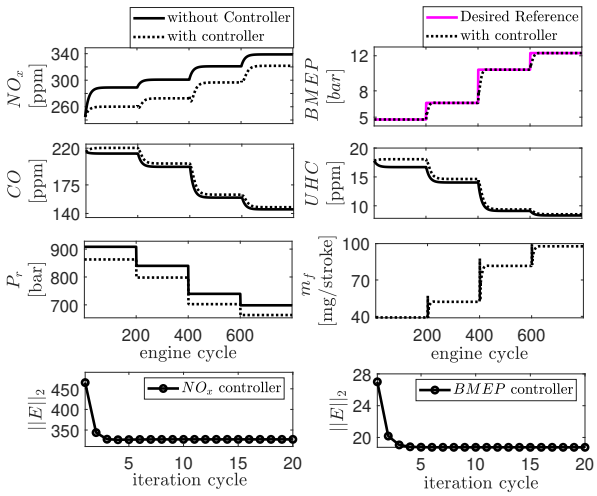

Fig. 6. NO_x Reduction system using plug-in PID and PD-type ILC - desired to reduce NO_x by 10 percent

provided with the target load, (BMEP), and a reduction of 5% of the open loop NO_x emission levels. The output of the ILC controller is the fuel rail pressure (P_r) and injected fuel amount (m_f). A constraint is then implemented in the ILC controller to prevent changes in the fuel rail pressure greater than 5%. This constraint is implemented to ensure that the emissions model remains accurate due to the range of data used to train the SVM-based COM and it is known that as fuel rail pressure is decreased an increase in particulate emissions is likely. Figure 5 compares the proposed ILC controller to the open-loop response. The engine-out emissions (NO_x, CO, and UHC) are also presented for the controller outputs (fuel rail pressure (P_r), and mass of fuel injected (m_f)).

The proposed ILC control strategy is able to learn from its previous error in load and NO_x reduction and the controller successfully reduces the NO_x emissions while meeting the BMEP target. However, this results in an increase in CO and UHC with the largest increase occurring at low loads, an increase of 2.03% and 4.95%, respectively. At the four loads tested the controller is able to successfully archive the target NO_x reduction of 5%.

Figure 5 also presents the convergence rate of the ILC controller as represented by the second norm of the error for both the load (BMEP) as well as the NO_x levels for the 800 engine cycles. The ILC controller presented has converged after 3 iterations of the applied load step. This result shows the quick convergence of the plug-in PD-type ILC controller presented.

With a target reduction of 5% NO_x, the fuel rail pressure is changed by under 5% for all loads. To explore if further NO_x reduction it is possible, the target is reduced to 10% of the open loop NO_x levels. This results in a greater reduction of NO_x but at the expense of increased UHC and CO levels as seen in Figure 6. Similar to the previous result, the greatest increase in CO and UHC occurs at the low load operating condition resulting in an increase of 3.25 and 8.20%, respectively. The controller is able to reach the desired BMEP targets for all 4 load cases and again the ILC controller converges within 3 interactions.

Now the reduction in NO_x is no longer constant between load points as was the case with a 5% reduction target. Figure 7 shows the relative change in emission levels for both a 5% and 10% NO_x reduction target. This figure shows that at low load operation there is a large change in emission levels where the 10% NO_x reduction results in 8.20% increase in UHC emissions at 4.7 bar BMEP. At high load operation, a larger NO_x reduction is possible with a smaller increase in CO and HC emissions.

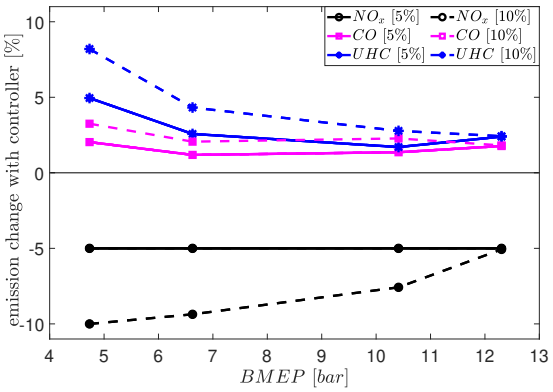

Fig. 7. NO_x Reduction vs CO and UHC change in steady state for both 5 % and 10 % NO_x reduction goals

The 5% limit on the change of rail pressure is the constraint for operation with a 10% NO_x reduction target as the controller is only able to achieve the desired reduction at low load operation. As the load increases the ILC controller is unable to meet the target NO_x reduction levels due to hitting this constraint. As discussed in this section and as shown in Figure 7, the developed control oriented emission and engine performance model provides insight into the

effect of engine operating parameters on different gaseous emissions and therefore can be used for future emissions trade-off studies. Depending on the emission level at each engine operating condition and the legislative requirements, the control strategy can make an informed decision to reduce one of the emissions while estimating the side-effect of its control actions on the other emissions. Therefore, the most appropriate control action can be carried out which simultaneously considers all of the emissions.

VI. CONCLUSIONS

The plug-in PD-type ILC controller developed in this paper shows the potential to reduce NO_x emission levels for repetitive load steps. In simulation, the controller is able to reduce NO_x levels while maintaining the desired engine load. This causes a slight increase in CO and UHC emission levels, a well-known emission trade-off. Here ILC is used to learn the best engine control inputs for load changes while reducing NO_x. This control strategy is applicable to diesel engines that are operated in repetitive load cycles. Experimental testing using the NO_x sensor to provide real-time emissions data to the controller as well as designing a plug-in ILC controller with a model-based controller such as a sliding mode or backstepping controller is the subject of our future work. Future measurements that include particulate measurement will be used to understand the impact of the proposed control strategy on particulate production.

REFERENCES

[1] Derong Liu, Ding Wang, and Hongliang Li. Decentralized stabilization for a class of continuous-time nonlinear interconnected systems using online learning optimal control approach. *IEEE transactions on neural networks and learning systems*, 25(2):418–428, 2014.

[2] Yong Yang, Lei Ma, and Deqing Huang. Development and repetitive learning control of lower limb exoskeleton driven by electrohydraulic actuators. *IEEE Transactions on Industrial Electronics*, 64(5):4169–4178, 2017.

[3] Jian-Xin Xu, Sanjib K Panda, and Tong Heng Lee. *Real-time iterative learning control: design and applications*. Springer Science & Business Media, 2008.

[4] Suguru Arimoto, Sadao Kawamura, and Fumio Miyazaki. Bettering operation of robots by learning. *Journal of Robotic systems*, 1(2):123–140, 1984.

[5] Craig Slepicka and Charles Robert Koch. Iterative learning on dual-fuel control of homogeneous charge compression ignition. *IFAC-PapersOnLine*, 49(11):347–352, 2016.

[6] Yan Liu and Xiaoe Ruan. Spatial iterative learning control for pitch of wind turbine. In *IEEE 7th Data Driven Control and Learning Systems Conference (DDCLS)*, pages 841–846. IEEE, 2018.

[7] Dong-Il Kim and Sungkwun Kim. An iterative learning control method with application for CNG machine tools. *IEEE Transactions on Industry Applications*, 32(1):66–72, 1996.

[8] He Li, Douglas A Bristow, and Robert G Landers. A plant-inversion based switched iterative learning control scheme for a special class of multivariable systems. In *ASME Dynamic Systems and Control Conference*, pages V001T01A008–V001T01A008. American Society of Mechanical Engineers, 2018.

[9] Qing-Yuan Xu and Xiao-Dong Li. Adaptive fuzzy ILC of nonlinear discrete-time systems with unknown dead zones and control directions. *International Journal of Systems Science*, pages 1–17, 2018.

[10] Jingxian Yu, Hui Dang, and Limin Wang. Fuzzy iterative learning control-based design of fault tolerant guaranteed cost controller for nonlinear batch processes. *International Journal of Control, Automation and Systems*, 16(5):2518–2527, 2018.

[11] Ali Madady, Hamid-Reza Reza-Alikhani, and Sara Zamiri. Optimal n-parametric type iterative learning control. *International Journal of Control, Automation and Systems*, 16(5):2187–2202, 2018.

[12] Timothy Johnson and Ameya Joshi. Review of vehicle engine efficiency and emissions. *SAE International Journal of Engins*, 11(6):1307–1330, 2018.

[13] Timothy V. Johnson. Review of vehicular emissions trends. *SAE Int. J. Engines*, 8, 04 2015.

[14] Alain Maiboom, Xavier Tauzia, and Jean-François Hétet. Experimental study of various effects of exhaust gas recirculation (EGR) on combustion and emissions of an automotive direct injection Diesel engine. *Energy*, 33(1):22–34, 2008.

[15] Khashayar Ebrahimi, Masoud Aliramezani, and Charles Robert Koch. An HCCI control oriented model that includes combustion efficiency. *IFAC-PapersOnLine*, 49(11):327–332, 2016.

[16] Zhiyu Han, Ali Uludogan, Gregory J Hampson, and Rolf D Reitz. Mechanism of soot and NOx emission reduction using multiple-injection in a diesel engine. *SAE transactions*, pages 837–852, 1996.

[17] Masoud Aliramezani, Charles Robert Koch, and Robert E Hayes. Estimating tailpipe NOx concentration using a dynamic NOx/ammonia cross sensitivity model coupled to a three state control oriented SCR model. *IFAC-PapersOnLine*, 49(11):8 – 13, 2016. 8th IFAC Symposium on Advances in Automotive Control AAC 2016.

[18] Xiukun Wei and Luigi Del Re. Gain scheduled H_∞ control for air path systems of diesel engines using LPV techniques. *IEEE transactions on control systems technology*, 15(3):406–415, 2007.

[19] Dezong Zhao, Cunjia Liu, Richard Stobart, Jiamei Deng, Edward Winward, and Guangyu Dong. An explicit model predictive control framework for turbocharged diesel engines. *IEEE Transactions on Industrial Electronics*, 61(7):3540–3552, 2013.

[20] Timothy V Johnson. Review of vehicular emissions trends. *SAE International Journal of Engines*, 8(3):1152–1167, 2015.

[21] Masoud Aliramezani, Charles Robert Koch, Robert E Hayes, and Ron Patrick. Amperometric solid electrolyte NOx sensors–the effect of temperature and diffusion mechanisms. *Solid State Ionics*, 313:7–13, 2017.

[22] C. Guardiola, J.J. López, J. Martín, and D. García-Sarmiento. Semiempirical in-cylinder pressure based model for NOx prediction oriented to control applications. *Applied Thermal Engineering*, 31(16):3275 – 3286, 2011.

[23] Masoud Aliramezani, Charles Robert Koch, and Ron Patrick. Phenomenological model of a solid electrolyte NOx and O2 sensor using temperature perturbation for on-board diagnostics. *Solid State Ionics*, 321:62 – 68, 2018.

[24] Masoud Aliramezani, Armin Norouzi, Charles Robert Koch, and Robert E Hayes. A control oriented diesel engine NOx emission model for on board diagnostics and engine control with sensor feedback. In *Proceedings of Combustion Institute - Canadian Section (CICS)*, 2019.

[25] Armin Norouzi, Masoud Aliramezani, and Charles Robert Koch. A correlation based model order reduction approach for a diesel engine NOx and BMEP dynamic model Using machine learning. *International Journal of Engine Research*, 2020.

[26] Jinchang Ren. Ann vs. SVM: Which one performs better in classification of MCCs in mammogram imaging. *Knowledge-Based Systems*, 26:144–153, 2012.

[27] Masoud Aliramezani, Armin Norouzi, and Charles Robert Koch. Support vector machine for a diesel engine performance and NOx emission control-oriented model. *IFAC-PapersOnLine, 21th IFAC World Congress*, 2020.

[28] Armin Norouzi, Khashayar Ebrahimi, and Charles Robert Koch. Integral discrete-time sliding mode control of homogeneous charge compression ignition (HCCI) engine load and combustion timing. *IFAC-PapersOnLine*, 52(5):153–158, 2019.

[29] Armin Norouzi and Charles Robert Koch. Integration of PD-type iterative learning control with adaptive sliding mode control. *IFAC-PapersOnLine, 21th IFAC World Congress*, 2020.

[30] Armin Norouzi and Charles Robert Koch. Robotic manipulator control using PD-type fuzzy iterative learning control. In *2019 IEEE Canadian Conference of Electrical and Computer Engineering (CCECE)*, pages 1–4, May 2019.

[31] David H Owens. *Iterative learning control: an optimization paradigm*. Springer, 2015.